

Network-level Cooperation in Random Access IoT Networks with Aggregators

Nikolaos Pappas¹, Ioannis Dimitriou², Zheng Chen³

¹Department of Science and Technology, Linköping University, Campus Norrköping, 60174, Sweden

² Department of Mathematics, University of Patras, 26500, Patras, Greece

³ Department of Electrical Engineering, Linköping University, 58183 Linköping, Sweden

Email: nikolaos.pappas@liu.se, idimit@math.upatras.gr, zheng.chen@liu.se

Abstract—In this work, we consider a random access IoT wireless network assisted by two aggregators. The nodes and the aggregators are transmitting in a random access manner under slotted time, the aggregators use network-level cooperation. We assume that all the nodes are sharing the same wireless channel to transmit their data to a common destination. The aggregators with out-of-band full duplex capability, are equipped with queues to store data packets that are transmitted by the network nodes and relaying them to the destination node. We characterize the throughput performance of the IoT network. In addition, we obtain the stability conditions for the queues at the aggregators and the average delay of the packets.

I. INTRODUCTION

The Internet of Things (IoT) is one of the most attractive concepts in the area of information and communication technology. IoT is expected to play an important role in our daily life by supporting massive connectivity with seamless service. It involves the interconnection of different, and possibly heterogeneous objects through the Internet using different communication technologies. The objects are equipped with communications capabilities and can vary from sensors, smart objects, etc. [1]–[3].

The total number of IoT connections is expected to grow tremendously the next years. The deployment of random access protocols in the IoT networks can potentially mitigate the congestion caused by massive amount of IoT devices with low signaling overhead [4]. To support the massive connectivity in future IoT networks, practical techniques are required to collect data from a large set of devices and the traditional orthogonal multi-access schemes are not sufficient. The works in [5]–[10] have considered data aggregation under different scenarios and setups and have evaluated the benefits of such technique.

Network-level cooperation introduced in [11] and [12] can be an effective alternative method for data aggregation. It is plain relaying without any physical layer considerations and it has been shown to provide large gain in terms of throughput and delay performance. Recently, several works have investigated relaying at the network level [13]–[21]. The deployment of aggregators under network-level cooperation can improve the throughput and delay in IoT networks [22]. However, due to the queueing delay, the stability conditions at the aggregator queues need to be considered.

In this work, we consider a random access IoT network with two aggregators which can receive and forward data

in form of packets from the network nodes. The nodes are transmitting in a random access manner under slotted time which is a common assumption in IoT technologies such as LoRa. The aggregators use network-level cooperation and their receiving and transmitting modules are operating in different bands, thus, they have out-of-band full duplex capabilities. Furthermore, we assume multi-packet reception (MPR) capabilities at the receivers. MPR is suitable to capture the SINR (Signal-to-Interference-plus-Noise-Ratio) based model and is more realistic to model the wireless transmission. Similar assumptions to our work can be found in [5], [9], [22].

The contributions of our work can be summarized as follows. Our primary goal is to address the problem of providing support for data collection in IoT networks by applying network-level cooperation. We provide the throughput analysis of the IoT network consisting of sensors that are assisted by two aggregators, from which we can gain insights on the scalability of the considered network. In addition, we study the stability conditions for the queues at the aggregators, which guarantee finite queueing delay. Furthermore, we study the average delay of the packets possibly received and forwarded by the aggregators. Our system is modeled as a two-dimensional discrete time Markov chain, and we show that the generating function of the stationary joint queue length distribution can be obtained by solving a fundamental functional equation with the theory of boundary value problems. The analysis in this work can act as a framework for other research directions that involve multiple aggregators with interacting queues.

The remainder of the paper is organized as follows: Section II describes the system model and in Section III we present the analysis related to the network-wide throughput. In Sections IV and V, we provide the analysis for the average delay per packet. The numerical evaluation of the theoretical results is presented in Section VI, and Section VII concludes the paper.

II. SYSTEM MODEL

A. Network Layer Model

We consider a wireless network consisting of M IoT nodes/sensors/objects, which intend to communicate to a common destination/sink D , and two aggregators, denoted by R_1 and R_2 , which can help aggregating and relaying messages from the IoT nodes to D . The network model is depicted in Fig. 1. The nodes are located in two non-overlapping regions. In the first region there are M_1 nodes, which are within the

service range of the aggregator R_1 . In the second region there are $M_2 = M - M_1$ nodes within the service range of the aggregator R_2 . Note that the transmissions in the first region cannot be overheard by the nodes in the second region and vice versa. This is a common assumption since there is planning for the placement of the aggregators in order to increase the coverage area without interfering with each other. *In the following, we will use the terms nodes, sensors, and objects interchangeably.*

The sensors intend to transmit packets to the destination node D and they are assumed to be saturated, i.e., they always have packets to transmit. In case the transmission from a sensor to D fails, the aggregator can help relaying the message to D and the aggregators do not generate their own traffic. We consider using *network-level cooperation* at the aggregators [11], [12], which means that the aggregators are cooperating as relays in a decode-and-forward manner. The packets are assumed to have equal length and the time is divided into slots, which corresponds to the transmission time of a packet. We assume that the sensors access the wireless channel randomly without any coordination among them. We consider a full multi-packet reception (MPR) channel model, which allows the receivers to successfully receive more than one packets when there are multiple transmissions in the same slot [23]. As the result, the sink node D can receive information simultaneously from the sensors and the aggregators. Note that when all nodes are transmitting, we can have in total up to M interfering devices at the sink. This assumption in the literature [5], [10], [22].

We assume that different frequency bands are allocated to the sensors and the aggregators, thus, there is no interference between them. On the other hand, the transmission of a node creates interference to the other nodes of the same kind, i.e., there is interference between the sensors, and between the aggregators. The transmitting and receiving units of the aggregators are operating in different channels/frequency bands to avoid self-interference, which can be considered as *out-of-band full duplex mode* [24]. The aggregators are equipped with queues that store possible packets from the sensors that failed to reach the destination. The queues are assumed to have infinite capacity, thus there is no packet dropping.¹ This is a common assumption in the literature, in the IoT context [22].

B. Physical Layer Model

At the beginning of a timeslot, sensor nodes that belong to the coverage area of R_i , attempt to transmit with probability t_i , $i = 1, 2$. The aggregator R_i will attempt to transmit a packet with probability α_i if it has a non-empty queue. Note that we assume that all the sensors in the same area transmit with the same probability. Our analysis can be easily extended to handle the general case where each node has different transmit probabilities.

¹In practice, the buffers have limited size, which is usually quite large. Our analysis based on the infinite buffer size assumption can capture this scenario with minor modifications. The arrival and service rates for the queues are defined in Section III.

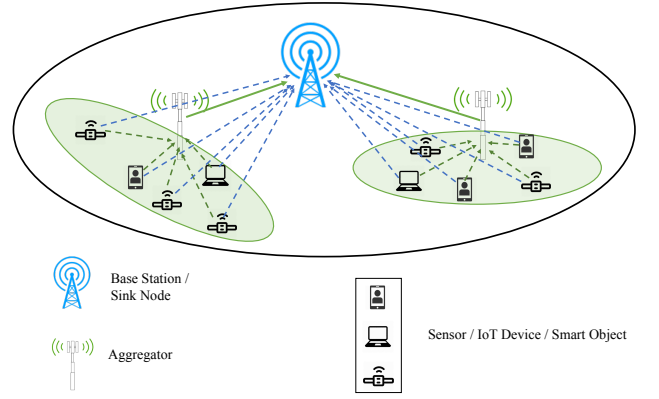


Fig. 1. The IoT network considered in this work. The nodes are assisted by two aggregators that are equipped with queues, and they are operating in an out-of-band full duplex mode.

The success probability between a sensor in the first coverage area and its aggregator is denoted by $P_i^{R_1}$, when there are i sensors from the same area transmitting in a timeslot. this success probability is the probability that the received SINR is greater than a threshold. The expression for this probability is omitted due to space limitation, and it can be found in [13]. Note that transmitting sensors from the other coverage area do not create interference at the aggregator. However, the concurrently transmitting sensors from both areas interfere with each other at the destination D . Denote by $P_{i,j}^{1D}$ the success probability to the sink from a sensor in coverage area 1 when there are i active transmitters from area 1 and j active transmitters from area 2. Similarly we can define $P_{i,j}^{2D}$.

A packet transmission from a sensor in the first area fails to reach the destination with probability $\bar{P}_{i,j}^{1D} = 1 - P_{i,j}^{1D}$, when there are i active sensors in the first area and j active sensors in the second area. In this case, that packet will be stored in the queue of aggregator R_1 with probability $P_i^{R_1}$. Otherwise, with probability $\bar{P}_i^{R_1}$, the aggregator fails to decode that packet and it has to be re-transmitted by the sensor in a future time slot.

Recall that if there are stored packets in the queues of the aggregator R_i , $i = 1, 2$, then R_i transmits a packet with probability α_i . If only one aggregator R_i is active, then the packet will be successfully transmitted to D with probability $p_{R_i, \{R_i\}}^D$. If both aggregators transmit simultaneously, then with probability $p_{R_i/R_1, R_2}^D$ the packet from R_i is successfully received by node D . If a transmitted packet from an aggregator fails to reach the D , that packet remains in the queue and will be retransmitted in a later time slot.

III. THROUGHPUT AND STABILITY ANALYSIS

In this section, we characterize the network throughput performance and provide the stability conditions for the queues at the aggregators.

A. Throughput Analysis

The throughput per node consists of the direct throughput from each sensor to the destination and the throughput contributed by the aggregator. Recall that the devices that are in

coverage from the first aggregator cannot cause interference at the receiver of the second aggregator. Moreover, the devices that are covered by the i -th aggregator, R_i , are transmitting with probability t_i , for $i = 1, 2$.

The direct throughput² from a sensor in the first coverage area to the sink is given by

$$T_{1,D} = \sum_{i=1}^{M_1} \sum_{j=0}^{M_2} \binom{M_1}{i-1} \binom{M_2}{j} t_1^i \bar{t}_1^{M_1-i} t_2^j \bar{t}_2^{M_2-j} P_{i,j}^{1D}. \quad (1)$$

The contributed throughput from a sensor to the aggregator in the first coverage area is given by

$$T_{1,R_1} = \sum_{i=1}^{M_1} \sum_{j=0}^{M_2} \binom{M_1}{i-1} \binom{M_2}{j} t_1^i \bar{t}_1^{M_1-i} t_2^j \bar{t}_2^{M_2-j} \bar{P}_{i,j}^{1D} P_i^{R_1}. \quad (2)$$

The total throughput seen by a sensor in the first coverage area is $T_1 = T_{1,D} + T_{1,R_1}$. Similarly, we can obtain the throughput seen by a sensor located in the second coverage area which is assisted by the second aggregator R_2 .

Then, we need to characterize the average arrival rates at the aggregators, denoted by λ_1 and λ_2 . Since we assume full MPR capability at the receivers, the i -th aggregator can receive up to N_i packets in a timeslot. We define $l_{k,i}$ as the probability that k packets will arrive in a timeslot at the i -th aggregator. The average arrival rate at the i -th aggregator is given by

$$\lambda_i = \sum_{k=1}^{M_i} k l_{k,i}, \quad i = 1, 2. \quad (3)$$

The probability $l_{k,1}$ where $1 \leq k \leq N_1$ is given by

$$l_{k,1} = \sum_{s=k}^{M_1} \sum_{m=0}^{M_2} \binom{M_1}{s} \binom{s}{k} \binom{M_2}{m} t_1^s \bar{t}_1^{M_1-s} t_2^m \bar{t}_2^{M_2-m} \times \left(\bar{P}_{s,m}^{1D} P_s^{R_1} \right)^k \left(P_{s,m}^{1D} + \bar{P}_{s,m}^{1D} \bar{P}_s^{R_1} \right)^{s-k}. \quad (4)$$

Similarly we can obtain $l_{k,2}$. The network-wide throughput is $T = M_1 T_1 + M_2 T_2$. The previous expressions for the throughput are valid when the queues at the aggregators are stable.³

B. Stability Analysis at the Aggregators

The average service rate for the aggregator i is given by

$$\mu_i = Pr(N_j \neq 0) \left[\alpha_i \bar{\alpha}_j p_{R_i, \{R_i\}}^D + \alpha_i \alpha_j p_{R_i, \{R_i, R_j\}}^D \right] + Pr(N_j = 0) \alpha_i p_{R_i, \{R_i\}}^D, \quad j = i \bmod 2 + 1, \quad (5)$$

where N_j is the queue size at queue j . The notation for the success probabilities used in (5) is the one introduced in Section II. We can easily see from (5) that the service rate of one queue depends on the status of the other queue. Thus,

²The direct throughput in this setup is equivalent to the throughput in the network without aggregators.

³Here we will not consider the case that the queues are not stable, but in order to obtain the throughput in this case one needs to replace the sum of expressions T_{i,R_i} with the service rate of the aggregator. In this case the network-wide throughput will be given by $T = M_1 T_{1,D} + M_2 T_{2,D} + \mu_1 + \mu_2$.

the queues are coupled. In order to bypass this difficulty we deploy the stochastic dominance technique introduced in [25]. The proof is along the lines of [20], [26] and is omitted due to space limitations. The stability conditions for the queues at the aggregators are described by the region $\mathcal{R} = \mathcal{R}_1 \cup \mathcal{R}_2$ where \mathcal{R}_i is given by (6).

IV. PRELIMINARY ANALYSIS

Let $N_{k,n}$ be the number of packets in the buffer of aggregator R_k , $k = 1, 2$, at the beginning of the n th slot. Then, $Y_n = (N_{1,n}, N_{2,n})$ is a discrete time Markov chain with state space $E = \{(i, j) : i, j = 0, 1, 2, \dots\}$. The queues of both aggregators evolve as follows:

$$N_{k,n+1} = [N_{k,n} + F_{k,n}]^+, \quad k = 1, 2, \quad (7)$$

where $F_{k,n}$ is the difference of the number of packets that enter the buffer of the k th aggregator at the beginning of slot n ($F_{k,n}$ equals 0 or ± 1), and $[x]^+ := \max(0, x)$.

Before proceeding with the analysis, we will slightly modify the notation for the success probabilities presented in Section II in order to be more convenient for the delay analysis. If two sensors transmit a packet simultaneously, $p_{i,\{1,2\}}^D$ represents the probability that the packet from sensor i is successfully received by node D and the packet from sensor $j = i \bmod 2 + 1$ failed to be received by D . $p_{1,2,\{1,2\}}^D$ represents the probability that the packets from both nodes are successfully received by D . Then we have $\bar{p}_{\{1,2\}}^D = 1 - p_{1,2,\{1,2\}}^D - p_{1,\{1,2\}}^D - p_{2,\{1,2\}}^D$, which denotes the probability that both packets fail to be received by the node D . If both aggregators transmit simultaneously, then with probability $p_{R_k, \{R_1, R_2\}}^D$ the packet from R_k is successfully received by node D , with probability $p_{R_1, R_2, \{R_1, R_2\}}^D$ the packets from both aggregators are successfully received by D , while with probability $\bar{p}_{\{R_1, R_2\}}^D = 1 - p_{R_1, R_2, \{R_1, R_2\}}^D - p_{R_1, \{R_1, R_2\}}^D - p_{R_2, \{R_1, R_2\}}^D$, both of them failed to be received by D .

Let $H(x, y)$ be the generating function of the joint stationary queue process,

$$H(x, y) = \lim_{n \rightarrow \infty} E(x^{N_{1,n}} y^{N_{2,n}}), \quad |x| \leq 1, |y| \leq 1.$$

Then, by exploiting (7) we obtain after lengthy calculations

$$R(x, y)H(x, y) = A(x, y)H(x, 0) + B(x, y)H(0, y) + C(x, y)H(0, 0), \quad (8)$$

where,

$$R(x, y) := 1 - L(x, y) \left[1 - \alpha_1 \hat{\alpha}_2 \left(1 - \frac{1}{x} \right) - \hat{\alpha}_1 \alpha_2 \left(1 - \frac{1}{y} \right) - \alpha_1 \alpha_2 p_{R_1, R_2, \{R_1, R_2\}}^D \right] \left(1 - \frac{1}{xy} \right),$$

$$\mathcal{R}_i = \left\{ (\lambda_1, \lambda_2) : \lambda_i \leq \alpha_i p_{R_i, \{R_i\}}^D - \frac{\alpha_i \alpha_j (p_{R_i, \{R_i\}}^D - p_{R_i/R_i, R_j}^D)}{\alpha_j \tilde{\alpha}_i p_{R_j, \{R_j\}}^D + \alpha_i \alpha_j p_{R_j/R_i, R_j}^D} \lambda_j, \lambda_j \leq \alpha_j \tilde{\alpha}_i p_{R_j, \{R_j\}}^D + \alpha_i \alpha_j p_{R_j/R_i, R_j}^D \right\}, \quad (6)$$

$$j = i \bmod 2 + 1.$$

is the *kernel* of the functional equation (8) and

$$\begin{aligned} A(x, y) &= L(x, y) \left[d_1 \left(1 - \frac{1}{x}\right) + \alpha_2 \hat{\alpha}_1 \left(1 - \frac{1}{y}\right) \right. \\ &\quad \left. + \alpha_1 \alpha_2 p_{R_1, R_2, \{R_1, R_2\}}^D \left(1 - \frac{1}{xy}\right) \right], \\ B(x, y) &= L(x, y) \left[d_2 \left(1 - \frac{1}{y}\right) + \alpha_1 \hat{\alpha}_2 \left(1 - \frac{1}{x}\right) \right. \\ &\quad \left. + \alpha_1 \alpha_2 p_{R_1, R_2, \{R_1, R_2\}}^D \left(1 - \frac{1}{xy}\right) \right], \\ C(x, y) &= L(x, y) \left[d_1 \left(\frac{1}{x} - 1\right) + d_2 \left(\frac{1}{y} - 1\right) \right. \\ &\quad \left. + \alpha_1 \alpha_2 p_{R_1, R_2, \{R_1, R_2\}}^D \left(\frac{1}{xy} - 1\right) \right], \\ L(x, y) &= 1 - (1 - x)t_1 [\bar{t}_2 \bar{p}_{1, \{1\}}^D p_{1, \{1\}}^{R_1} \\ &\quad + t_2 (\bar{p}_{1, \{2\}}^D + p_{2, \{1, 2\}}^D) p_{1, \{1, 2\}}^{R_1} \\ &\quad + (1 - y)t_2 [\bar{t}_1 \bar{p}_{2, \{2\}}^D p_{2, \{2\}}^{R_2} \\ &\quad + t_1 (\bar{p}_{1, \{2\}}^D + p_{1, \{1, 2\}}^D) p_{1, \{1, 2\}}^{R_2} \\ &\quad + (1 - x)(1 - y)t_1 t_2 \bar{p}_{1, \{2\}}^D p_{1, \{1, 2\}}^{R_1} p_{2, \{1, 2\}}^{R_2}], \\ \hat{\alpha}_k &= \tilde{\alpha}_k p_{R_k, \{R_k\}}^D + \alpha_k p_{R_k, \{R_1, R_2\}}^D, \quad k = 1, 2, \\ d_1 &= \alpha_1 (\hat{\alpha}_2 - p_{R_1, \{R_1\}}^D), \\ d_2 &= \alpha_2 (\hat{\alpha}_1 - p_{R_2, \{R_2\}}^D). \end{aligned}$$

Clearly, for every fixed y with $|y| \leq 1$, $H(x, y)$ it is regular in x for $|x| < 1$, and continuous in x for $|x| \leq 1$; similar observation hold for the variable y .

Some interesting relations are directly obtained using (8). In particular, by setting in (8) $y = 1$, dividing with $x - 1$, and taking the limit $x \rightarrow 1$, by using the L'Hospital rule, and vice-versa we obtain the following conservation of flow relations:

$$\begin{aligned} \lambda_1 &= \alpha_1 \tilde{\alpha}_2 [1 - H(1, 0) - H(0, 1) + H(0, 0)] \\ &\quad + \alpha_1 p_{R_1, \{R_1\}}^D [H(1, 0) - H(0, 0)], \\ \lambda_2 &= \alpha_2 \tilde{\alpha}_1 [1 - H(1, 0) - H(0, 1) + H(0, 0)] \\ &\quad + \alpha_2 p_{R_2, \{R_2\}}^D [H(0, 1) - H(0, 0)], \end{aligned} \quad (9)$$

where, $\tilde{\alpha}_k := \hat{\alpha}_k + \alpha_k p_{R_1, R_2, \{R_1, R_2\}}^D$, $k = 1, 2$,

$$\begin{aligned} \lambda_1 &:= t_1 \bar{t}_2 \bar{p}_{1, \{1\}}^D p_{1, \{1\}}^{R_1} + t_1 t_2 (\bar{p}_{1, \{2\}}^D + p_{2, \{1, 2\}}^D) p_{1, \{1, 2\}}^{R_1}, \\ \lambda_2 &:= t_2 \bar{t}_1 \bar{p}_{2, \{2\}}^D p_{2, \{2\}}^{R_2} + t_1 t_2 (\bar{p}_{1, \{2\}}^D + p_{1, \{1, 2\}}^D) p_{2, \{1, 2\}}^{R_2}. \end{aligned}$$

Note that the previous equations are the same with the ones obtained in the previous section, but here we use the more convenient notation for the delay analysis regarding the success probabilities. In order to facilitate the presentation we present the case of two nodes, but clearly the analysis holds for the general case of N nodes, just by replacing the right parts of λ_1 and λ_2 .

Equations (9), equate the flow of jobs into an aggregator, with the flow of jobs out of the aggregator. Looking carefully at (9) it is readily seen that the following analysis is distinguished in two cases:

$$\begin{aligned} 1) \quad &\frac{\alpha_1 \tilde{\alpha}_2}{\alpha_1 p_{R_1, \{R_1\}}^D} + \frac{\alpha_2 \tilde{\alpha}_1}{\alpha_2 p_{R_2, \{R_2\}}^D} = 1. \text{ Then,} \\ &H(0, 0) = 1 - \frac{\lambda_1}{\alpha_1 p_{R_1, \{R_1\}}^D} - \frac{\lambda_2}{\alpha_2 p_{R_2, \{R_2\}}^D} = 1 - \rho. \end{aligned}$$

2) $\frac{\alpha_1 \tilde{\alpha}_2}{\alpha_1 p_{R_1, \{R_1\}}^D} + \frac{\alpha_2 \tilde{\alpha}_1}{\alpha_2 p_{R_2, \{R_2\}}^D} \neq 1$. Then, (9) yields

$$\begin{aligned} H(1, 0) &= \frac{\alpha_1 \tilde{\alpha}_2 (\lambda_2 - \alpha_2 p_{R_2, \{R_2\}}^D) - \tilde{d}_2 (\lambda_1 + H(0, 0) \alpha_1 p_{R_1, \{R_1\}}^D)}{\tilde{d}_1 \tilde{d}_2 - \alpha_1 \alpha_2 \tilde{\alpha}_1 \tilde{\alpha}_2}, \\ H(0, 1) &= \frac{\alpha_2 \tilde{\alpha}_1 (\lambda_1 - \alpha_1 p_{R_1, \{R_1\}}^D) - \tilde{d}_1 (\lambda_2 + H(0, 0) \alpha_2 p_{R_2, \{R_2\}}^D)}{\tilde{d}_1 \tilde{d}_2 - \alpha_1 \alpha_2 \tilde{\alpha}_1 \tilde{\alpha}_2}, \end{aligned}$$

$$\text{where } \tilde{d}_1 = \alpha_1 (\tilde{\alpha}_2 - p_{R_1, \{R_1\}}^D), \quad \tilde{d}_2 = \alpha_2 (\tilde{\alpha}_1 - p_{R_2, \{R_2\}}^D).$$

A. Kernel analysis

The kernel $R(x, y)$ plays a crucial role in the following analysis and here we provide some important properties. For convenience, assume in the following that $p_{R_1, R_2, \{R_1, R_2\}}^D = 0$. It is readily seen that

$$R(x, y) = a(x)y^2 + b(x)y + c(x) = \hat{a}(y)x^2 + \hat{b}(y)x + \hat{c}(y),$$

where, for $L = t_1 t_2 \bar{p}_{1, \{2\}}^D p_{1, \{1, 2\}}^{R_1} p_{2, \{1, 2\}}^{R_2}$,

$$\begin{aligned} \hat{a}(y) &= L(1 - \alpha_1 \hat{\alpha}_2 - \alpha_2 \hat{\alpha}_1)y^2 + y[\lambda_1(a_1 \hat{\alpha}_2 + \alpha_2 \hat{\alpha}_1 - 1) \\ &\quad + L(\alpha_1 \hat{\alpha}_2 + 2\alpha_2 \hat{\alpha}_1 - 1)] - \alpha_2 \hat{\alpha}_1 (\lambda_1 + L), \\ \hat{b}(y) &= y^2[\lambda_2(\alpha_1 \hat{\alpha}_2 + \alpha_2 \hat{\alpha}_1 - 1) + L(2\alpha_1 \hat{\alpha}_2 + \alpha_2 \hat{\alpha}_1 - 1)] \\ &\quad + y[\lambda_1(1 - 2\alpha_1 \hat{\alpha}_2 - \alpha_2 \hat{\alpha}_1) + \lambda_2(1 - 2\hat{\alpha}_1 \alpha_2 - \alpha_1 \hat{\alpha}_2) \\ &\quad + L(1 - 2(\hat{\alpha}_1 \alpha_2 + \alpha_1 \hat{\alpha}_2)) + \alpha_1 \hat{\alpha}_2 + \alpha_2 \hat{\alpha}_1] \\ &\quad + \hat{\alpha}_1 \alpha_2 (\lambda_1 + \lambda_2 + L - 1), \\ \hat{c}(y) &= \alpha_1 \hat{\alpha}_2 y[\lambda_1 - 1 + (\lambda_2 + L)(1 - y)], \\ a(x) &= L(1 - \alpha_1 \hat{\alpha}_2 - \alpha_2 \hat{\alpha}_1)x^2 + x[\lambda_2(\alpha_1 \hat{\alpha}_2 + \alpha_2 \hat{\alpha}_1 - 1) \\ &\quad + L(2\alpha_1 \hat{\alpha}_2 + \alpha_2 \hat{\alpha}_1 - 1)] - \alpha_1 \hat{\alpha}_2 (\lambda_2 + L), \\ b(x) &= x^2[\lambda_1(\alpha_1 \hat{\alpha}_2 + \alpha_2 \hat{\alpha}_1 - 1) + L(2\alpha_2 \hat{\alpha}_1 + \alpha_1 \hat{\alpha}_2 - 1)] \\ &\quad + x[\lambda_1(1 - 2\alpha_1 \hat{\alpha}_2 - \alpha_2 \hat{\alpha}_1) + \lambda_2(1 - 2\hat{\alpha}_1 \alpha_2 - \alpha_1 \hat{\alpha}_2) \\ &\quad + L(1 - 2(\hat{\alpha}_1 \alpha_2 + \alpha_1 \hat{\alpha}_2)) + \alpha_1 \hat{\alpha}_2 + \alpha_2 \hat{\alpha}_1] \\ &\quad + \hat{\alpha}_2 \alpha_1 (\lambda_1 + \lambda_2 + L - 1), \\ c(x) &= \alpha_2 \hat{\alpha}_1 x[\lambda_2 - 1 + (\lambda_1 + L)(1 - x)]. \end{aligned}$$

The roots of $R(x, y) = 0$ are $X_{\pm}(y) = \frac{-\hat{b}(y) \pm \sqrt{D_y(y)}}{2\hat{a}(y)}$, $Y_{\pm}(x) = \frac{-b(x) \pm \sqrt{D_x(x)}}{2a(x)}$, where $D_y(y) = \hat{b}(y)^2 - 4\hat{a}(y)\hat{c}(y)$, $D_x(x) = b(x)^2 - 4a(x)c(x)$.

Lemma IV.1. For $|y| = 1$, $y \neq 1$, $R(x, y) = 0$ has exactly one root $x = X_0(y)$ such that $|X_0(y)| < 1$. When $\lambda_1 < \alpha_1 \hat{\alpha}_2$, $X_0(1) = 1$. Similarly, $R(x, y) = 0$ has exactly one root $y = Y_0(x)$, such that $|Y_0(x)| \leq 1$, for $|x| = 1$.

Proof. See Appendix A. \square

The lemma below provides information about the location of the branch points of the two-valued functions $Y(x)$, $X(y)$, its proof is based on algebraic arguments, thus it is omitted.

Lemma IV.2. The algebraic function $Y(x)$, defined by $R(x, Y(x)) = 0$, has four real branch points $0 < x_1 < x_2 \leq 1 < x_3 < x_4$. Moreover, $D_x(x) < 0$, $x \in (x_1, x_2) \cup (x_3, x_4)$ and $D_x(x) > 0$, $x \in (-\infty, x_1) \cup (x_2, x_3) \cup (x_4, \infty)$.

Similarly, $X(y)$, is defined by $R(X(y), y) = 0$, it has four real branch points $0 \leq y_1 < y_2 \leq 1 < y_3 < y_4$, and $D_x(y) < 0$, $y \in (y_1, y_2) \cup (y_3, y_4)$ and $D_x(y) > 0$, $y \in (-\infty, y_1) \cup (y_2, y_3) \cup (y_4, \infty)$.

Let $\tilde{C}_x = \mathbb{C}_x - ([x_1, x_2] \cup [x_3, x_4])$, $\tilde{C}_y = \mathbb{C}_y - ([y_1, y_2] \cup [y_3, y_4])$, where \mathbb{C}_x , \mathbb{C}_y the complex planes of x , y , respectively. In \tilde{C}_x (resp. \tilde{C}_y), denote by $Y_0(x)$ (resp. $X_0(y)$) the root of $R(x, Y(x)) = 0$ (resp. $R(X(y), y) = 0$) with the smallest modulus, and $Y_1(x)$ (resp. $X_1(y)$) the other one. Define the image contours, $\mathcal{L} = Y_0[\overrightarrow{x_1, x_2}]$, $\mathcal{M} = X_0[\overrightarrow{y_1, y_2}]$, where $\overrightarrow{[u, v]}$ stands for the contour traversed from u to v along the upper edge of the slit $[u, v]$ and then back to u along the lower edge of the slit. In the following lemma we provide exact characterization for the smooth and closed contours \mathcal{L} , \mathcal{M} respectively:

Lemma IV.3. *The algebraic function $X(y)$, $y \in [y_1, y_2]$ lies on a closed contour \mathcal{M} , which is symmetric with respect to the real line and defined by*

$$|x|^2 = m(\operatorname{Re}(x)), \quad m(\delta) = \frac{\widehat{c}(\zeta(\delta))}{\widehat{a}(\zeta(\delta))}, \quad |x|^2 \leq \frac{\widehat{c}(y_2)}{\widehat{a}(y_2)},$$

where, $\zeta(\delta) = \frac{k_2(\delta) - \sqrt{k_2^2(\delta) - 4k_3(\delta)k_1(\delta)}}{2k_1(\delta)}$, and

$$\begin{aligned} k_1(\delta) &:= a_1\widehat{a}_2(\lambda_2 + 2L(1 - \delta)) \\ &\quad - (\lambda_2 + L(1 - 2\delta))(1 - \widehat{a}_1a_2), \\ k_2(\delta) &:= 2\delta[a_1\widehat{a}_2(\lambda_1 + L) + \widehat{a}_1a_2(\lambda_1 + 2L) \\ &\quad - \lambda_1 - L] + \lambda_1 + \lambda_2 + L + a_1\widehat{a}_2(1 - 2\lambda_1) \\ &\quad + \widehat{a}_1a_2(1 - \lambda_1 - 2(\lambda_2 + L)), \\ k_3(\delta) &:= -[\lambda_2(\widehat{a}_1a_2 + a_1\widehat{a}_2) \\ &\quad + \widehat{a}_1a_2(1 + (\lambda_1 + L)(1 + 2\delta))]. \end{aligned}$$

Moreover, $\beta_0 := \sqrt{\frac{\widehat{c}(y_2)}{\widehat{a}(y_2)}}$, $\beta_1 := -\sqrt{\frac{\widehat{c}(y_1)}{\widehat{a}(y_1)}}$ are the extreme right and left points of \mathcal{M} , respectively. Similarly, $Y(x)$, $x \in [x_1, x_2]$ lies on a closed contour \mathcal{L} . Its exact representation is derived as for \mathcal{M} , and further details are omitted.

Proof. See Appendix B. \square

B. The boundary value problems

Here, we proceed with the derivation of the probability generating function of the joint stationary queue length distribution at relays. The analysis is distinguished in two cases according to the values of the parameters.

1) *A Dirichlet boundary value problem:* Let $\frac{a_1\widehat{a}_2}{a_1p_{R_1, \{R_1\}}^D} + \frac{a_2\widehat{a}_1}{a_2p_{R_2, \{R_2\}}^D} = 1$. It can be easily seen that

$$A(x, y) = \frac{d_1}{\alpha_1\widehat{\alpha}_2}B(x, y) \Leftrightarrow A(x, y) = \frac{\alpha_2\widehat{\alpha}_1}{d_2}B(x, y).$$

Therefore, for $y \in \mathcal{D}_y = \{y \in \mathcal{C} : |y| \leq 1, |X_0(y)| \leq 1\}$,

$$\alpha_2\widehat{\alpha}_1H(X_0(y), 0) + d_2H(0, y) + \frac{\alpha_2\widehat{\alpha}_1(1-\rho)C(X_0(y), y)}{A(X_0(y), y)} = 0. \quad (10)$$

Both $H(X_0(y), 0)$, and $H(0, y)$, where $y \in \mathcal{D}_y - [y_1, y_2]$, are analytic functions. Using analytic continuation arguments we consider (10) for $x \in \mathcal{M}$

$$\alpha_2\widehat{\alpha}_1H(x, 0) + d_2H(0, Y_0(x)) + \frac{\alpha_2\widehat{\alpha}_1(1-\rho)C(x, Y_0(x))}{A(x, Y_0(x))} = 0. \quad (11)$$

By noticing that $H(0, Y_0(x))$ is real for $x \in \mathcal{M}$, i.e., $Y_0(x) \in [y_1, y_2]$, we have

$$\operatorname{Re}(iH(x, 0)) = w(x), \quad x \in \mathcal{M}, \quad (12)$$

where $w(x) := \operatorname{Re}(-i\frac{C(x, Y_0(x))}{A(x, Y_0(x))})(1 - \rho)$. Clearly, some technical requirements are needed to be everything well defined. In particular, we have to investigate the possible poles of $H(x, 0)$, $x \in S := G_{\mathcal{M}} \cap \bar{D}_x^c$, where $G_{\mathcal{U}}$ be the interior domain bounded by \mathcal{U} , and $D_x = \{x : |x| < 1\}$, $\bar{D}_x = \{x : |x| \leq 1\}$, $\bar{D}_x^c = \{x : |x| > 1\}$. This is equivalent with the investigation of the zeros of $A(x, Y_0(x))$, $x \in S_x$. Moreover, in order to solve (12) we first transform the problem from \mathcal{M} to the unit circle; see Appendix C for details. Let the conformal mapping, $z = \gamma(x) : G_{\mathcal{M}} \rightarrow G_{\mathcal{C}}$, and its inverse $x = \gamma_0(z) : G_{\mathcal{C}} \rightarrow G_{\mathcal{M}}$.

By applying the transformation, the problem is reduced to the determination of function $\tilde{T}(z) = H(\gamma_0(z), 0)$ regular for $z \in G_{\mathcal{C}}$, continuous for $z \in \mathcal{C} \cup G_{\mathcal{C}}$ such that, $\operatorname{Re}(i\tilde{T}(z)) = w(\gamma_0(z))$, $z \in \mathcal{C}$. The solution of the Dirichlet problem with boundary condition (12) is:

$$H(x, 0) = -\frac{1-\rho}{2\pi} \int_{|t|=1} f(t) \frac{t+\gamma(x)}{t-\gamma(x)} \frac{dt}{t} + C, \quad x \in \mathcal{M}, \quad (13)$$

where $f(t) = \operatorname{Re}(-i\frac{C(\gamma_0(t), Y_0(\gamma_0(t)))}{A(\gamma_0(t), Y_0(\gamma_0(t)))})$, C a constant to be defined by setting $x = 0 \in G_{\mathcal{M}}$ in (13) and using the fact that $H(0, 0) = 1 - \rho$, $\gamma(0) = 0$ (In case $H(x, 0)$ has a pole, say \bar{x} , we still have a Dirichlet problem for the function $(x - \bar{x})H(x, 0)$). Setting $t = e^{i\phi}$, $\gamma_0(e^{i\phi}) = \rho(\psi(\phi))e^{i\psi(\phi)}$, we obtain after some algebra,

$$f(e^{i\phi}) = \frac{d_1\alpha_2 \sin(\psi(\phi))(1 - Y_0(\gamma_0(e^{i\phi})))^{-1}}{\rho(\psi(\phi))k(\phi)},$$

which is an odd function of ϕ , and

$$\begin{aligned} k(\phi) &= [\alpha_2\widehat{\alpha}_1(1 - Y_0^{-1}(\gamma_0(e^{i\phi}))) + d_1(1 - \frac{\cos(\psi(\phi))}{\rho(\psi(\phi))})]^2 \\ &\quad + (d_1 \frac{\sin(\psi(\phi))}{\rho(\psi(\phi))})^2. \end{aligned}$$

Thus, $C = 1 - \rho$. Substituting in (13) we obtain after simple calculations an integral representation of $H(x, 0)$ on a real interval for $x \in G_{\mathcal{M}}$, i.e.,

$$H(x, 0) = (1 - \rho) \left\{ 1 + \frac{2\gamma(x)i}{\pi} \int_0^\pi \frac{f(e^{i\phi}) \sin(\phi) d\phi}{1 - 2\gamma(x) \cos(\phi) - \gamma(x)^2} \right\}. \quad (14)$$

Similarly, we can determine $H(0, y)$ by solving another Dirichlet boundary value problem on the closed contour \mathcal{L} . Then, using the fundamental functional equation (8) we uniquely obtain $H(x, y)$.

2) *A homogeneous Riemann-Hilbert boundary value problem:* In case $\frac{a_1\widehat{a}_2}{a_1^*p_{R_1, \{R_1\}}^D} + \frac{a_2\widehat{a}_1}{a_2^*p_{R_2, \{R_2\}}^D} \neq 1$, consider the following transformation:

$$\begin{aligned} G(x) &:= H(x, 0) + \frac{\alpha_1 p_{R_1, \{R_1\}}^D d_2 H(0, 0)}{d_1 d_2 - \alpha_1 \widehat{\alpha}_2 \alpha_2 \widehat{\alpha}_1}, \\ L(y) &:= H(0, y) + \frac{\alpha_2 p_{R_2, \{R_2\}}^D d_1 H(0, 0)}{d_1 d_2 - \alpha_1 \widehat{\alpha}_2 \alpha_2 \widehat{\alpha}_1}. \end{aligned}$$

Then, for $y \in \mathcal{D}_y$,

$$A(X_0(y), y)G(X_0(y)) = -B(X_0(y), y)L(y). \quad (15)$$

Using similar arguments as in previous subsection, we have for $x \in \mathcal{M}$

$$A(x, Y_0(x))G(x) = -B(x, Y_0(x))L(Y_0(x)). \quad (16)$$

Clearly, $G(x)$ is holomorphic in D_x , continuous in \bar{D}_x , but it might have poles in S_x , based on the values of the system parameters. These poles, if exist, coincide with the zeros of $A(x, Y_0(x))$ in S_x . For $y \in [y_1, y_2]$, let $X_0(y) = x \in \mathcal{M}$ and realize that $Y_0(X_0(y)) = y$ so that $y = Y_0(x)$. Taking into account the possible poles of $G(x)$, and noticing that $L(Y_0(x))$ is real for $x \in \mathcal{M}$, since $Y_0(x) \in [y_1, y_2]$, we have

$$Re[iU(x)\tilde{G}(x)] = 0, x \in \mathcal{M}, \quad (17)$$

$$U(x) = \frac{A(x, Y_0(x))}{(x-\bar{x})^r B(x, Y_0(x))}, \tilde{G}(x) = (x-\bar{x})^r G(x),$$

where $r = 0, 1$, whether \bar{x} is zero or not of $A(x, Y_0(x))$ in S_x . Thus, $\tilde{G}(x)$ is regular for $x \in G_{\mathcal{M}}$, continuous for $x \in \mathcal{M} \cup G_{\mathcal{M}}$, and $U(x)$ is a non-vanishing function on \mathcal{M} . By conformally transform the problem (17) from \mathcal{M} to the unit circle, using $z = \gamma(x) : G_{\mathcal{M}} \rightarrow G_{\mathcal{C}}$, and its inverse given by $x = \gamma_0(z) : G_{\mathcal{C}} \rightarrow G_{\mathcal{M}}$, the problem in (17) is reduced to the following: find a function $F(z) := \tilde{G}(\gamma_0(z))$, regular in $G_{\mathcal{C}}$, continuous in $G_{\mathcal{C}} \cup \mathcal{C}$ such that, $Re[iU(\gamma_0(z))F(z)] = 0, z \in \mathcal{C}$.

We now need additional information in order to derive a solution for the above problem, i.e., we must determine the index $\chi = \frac{-1}{\pi} [arg\{U(x)\}]_{x \in \mathcal{M}}$, where $[arg\{U(x)\}]_{x \in \mathcal{M}}$, denotes the variation of the argument of the function $U(x)$ as x moves along the closed contour \mathcal{M} in the positive direction, provided that $U(x) \neq 0, x \in \mathcal{M}$. Following the methodology in [27], the value of the index is closely related to the stability conditions. The following lemma provides the necessary information.

Lemma IV.4. 1) If $\lambda_2 < \alpha_2 \hat{\alpha}_1$, then $\chi = 0$ is equivalent to

$$\frac{dA(x, Y_0(x))}{dx} \Big|_{x=1} < 0 \Leftrightarrow \lambda_1 < \alpha_1 p_{R_1, \{R_1\}}^D + \frac{d_1 \lambda_2}{\alpha_2 \hat{\alpha}_1},$$

$$\frac{dB(X_0(y), y)}{dy} \Big|_{y=1} < 0 \Leftrightarrow \lambda_2 < \alpha_2 p_{R_2, \{R_2\}}^D + \frac{d_2 \lambda_1}{\alpha_1 \hat{\alpha}_2}.$$

2) If $\lambda_2 \geq \alpha_2 \hat{\alpha}_1$, $\chi = 0$ is equivalent to

$$\frac{dB(X_0(y), y)}{dy} \Big|_{y=1} < 0 \Leftrightarrow \lambda_2 < \alpha_2 p_{R_2, \{R_2\}}^D + \frac{d_2 \lambda_1}{\alpha_1 \hat{\alpha}_2}.$$

Thus, under stability conditions the problem defined in (17) has a unique solution for $x \in G_{\mathcal{M}}$ given by,

$$H(x, 0) = \frac{K(x-\bar{x})^{-r} \exp[\frac{1}{2i\pi} \int_{|t|=1} \frac{\log\{J(t)\}}{t-\gamma(x)} dt]}{-\frac{\alpha_1 p_{R_1, \{R_1\}}^D d_2 H(0,0)}{d_1 d_2 - \alpha_1 \hat{\alpha}_2 \alpha_2 \hat{\alpha}_1}}, \quad (18)$$

where K is a constant and $J(t) = \frac{\bar{U}_1(t)}{U_1(t)}$, $U_1(t) = U(\gamma_0(t))$, $|t| = 1$. Setting $x = 0$ in (18) we derive a relation between K and $H(0, 0)$. Then, for $x = 1 \in G_{\mathcal{M}}$, and using the first in (9) we can obtain K and $H(0, 0)$. Substituting back in (18) we obtain for $x \in G_{\mathcal{M}}$,

$$H(x, 0) = \frac{\lambda_1 d_2 + \alpha_1 \hat{\alpha}_2 (\bar{t}_1 \bar{t}_2 \alpha_2 p_{R_2, \{R_2\}}^D - \lambda_2)}{(\bar{x}-1)^r t_1 t_2 (\alpha_1 \hat{\alpha}_2 \alpha_2 \hat{\alpha}_1 - d_1 d_2)} \left((\bar{x}-x)^r \exp[\frac{\gamma(x)-\gamma(1)}{2i\pi} \int_{|t|=1} \frac{\log\{J(t)\}}{(t-\gamma(x))(t-\gamma(1))} dt] \right. \\ \left. + \frac{\alpha_1 p_{R_1, \{R_1\}}^D d_2 \bar{x}^r}{\alpha_1 \hat{\alpha}_2 \alpha_2 p_{R_2, \{R_2\}}^D} \exp[\frac{-\gamma(1)}{2i\pi} \int_{|t|=1} \frac{\log\{J(t)\}}{t(t-\gamma(1))} dt] \right). \quad (19)$$

The other unknown function $H(0, y)$ is determined similarly, by solving another Riemann-Hilbert boundary value problem

on the closed contour \mathcal{L} . Then, using the fundamental functional equation (8) we uniquely obtain $H(x, y)$.

Having obtained the $H(x, y)$ several performance metrics can be obtained. In particular, using Little's law, the expected delay at each aggregator equals

$$D_1 = \frac{\lambda_1 + d_1 H_1(1, 0)}{\lambda_1 \alpha_1 \hat{\alpha}_2}, D_2 = \frac{\lambda_2 + d_2 H_2(0, 1)}{\lambda_2 \alpha_2 \hat{\alpha}_1},$$

where $H_1(1, 0) := \frac{d}{dx} H(x, 0)|_{x=1}$, and $H_2(0, 1) := \frac{d}{dy} H(0, y)|_{y=1}$.

V. EXPLICIT BOUNDS FOR THE MEAN DELAY IN THE SYMMETRICAL SYSTEM

In the following we consider the symmetrical model and obtain explicit bounds for the average delay. In particular, for $k = 1, 2$ let $\alpha_k = \alpha$, $t_k = t$, $p_{k, \{k\}}^{R_k} = s_1^R$, $p_{k, \{k\}}^D = s_1^D$, $p_{k, \{1, 2\}}^{R_k} = s_2^R$, $p_{k, \{1, 2\}}^D = s_2^D$, $p_{1, 2, \{1, 2\}}^D = s_0^D$, $p_{R_k, \{R_k\}}^D = r_1^D$, $p_{R_k, \{R_1, R_2\}}^D = r_2^D$, $p_{R_1, R_2, \{R_1, R_2\}}^D = r_0^D$, and as a result $d_k = d := \alpha^2 (r_2^D - r_1^D)$. Note that due to the symmetry, $H(0, 1) = H(1, 0)$. Using the fact that $H(1, 1) = 1$, and setting in (8) $y = 1$, dividing with $x - 1$, and taking the limit $x \rightarrow 1$, by using the L'Hospital rule,

$$\alpha[\hat{\alpha} + \alpha r_0^D] - \lambda = \frac{(d + \alpha \hat{\alpha} + 2\alpha^2 r_0^D)H(1, 0)}{-(d + \alpha^2 r_0^D)H(0, 0)}, \quad (20)$$

where now due to the symmetry $\lambda_k = \lambda$, $k = 1, 2$, $\hat{\alpha} = \bar{\alpha} r_1^D + \alpha r_2^D$, and

$$\lambda = t^2 s_2^R (\bar{s}_0^D + s_2^D) + t \bar{s}_1^D s_1^R.$$

Note that $\alpha[\hat{\alpha} + \alpha r_0^D] > \lambda$ due to the stability condition.

Denote by $H_1(x, y)$, $H_2(x, y)$ the derivatives of $H(x, y)$ with respect to x, y . Due to the symmetry, $H_1(1, 1) = H_2(1, 1)$, $H_1(1, 0) = H_2(0, 1)$. Denote by $M_k = H_1(1, 1)$, $k = 1, 2$. Differentiating (8) with respect to x , setting $(x, y) = (1, 1)$, and using (20) we obtain

$$M_1 = \frac{\lambda \bar{\lambda} + (d + \alpha^2 r_0^D)H_1(1, 0)}{\alpha[\hat{\alpha} + \alpha r_0^D] - \lambda}, \quad (21)$$

where $\bar{\lambda} = 1 - \lambda$. Now set $x = y$ in (8) we obtain

$$2(\alpha[\hat{\alpha} + \alpha r_0^D] - \lambda) \frac{d}{dx} H(x, x)|_{x=1} = 2(1 + 2\lambda)(\alpha[\hat{\alpha} + \alpha r_0^D] - \lambda) + \alpha^2 r_0^D P(N_1 > 0, N_2 > 0) + 2H_1(1, 0)(d + \alpha \hat{\alpha} + 2\alpha^2 r_0^D) - 2\alpha(\hat{\alpha} + \alpha r_0^D) + t^2 \bar{s}_0^D (s_2^R)^2 + 4\lambda(1 - \alpha \hat{\alpha} - \alpha^2 r_0^D). \quad (22)$$

Using (21), (22), and realizing that due to the symmetry $\frac{d}{dx} H(x, x)|_{x=1} = 2M_1$, we obtain

$$M_1 = M_2 = \frac{\lambda \bar{\lambda} (d + \alpha \hat{\alpha} + 2\alpha^2 r_0^D)}{2\alpha(\alpha[\hat{\alpha} + \alpha r_0^D] - \lambda)} - \frac{(d + \alpha^2 r_0^D)[2\lambda(1 + 2\lambda) + t^2 \bar{s}_0^D (s_2^R)^2 + \alpha^2 r_0^D P(N_1 > 0, N_2 > 0)]}{2\alpha(\alpha[\hat{\alpha} + \alpha r_0^D] - \lambda)}. \quad (23)$$

Using Little's law, the average delay at each aggregator is

$$D_1 = D_2 := S - \phi, \quad (24)$$

where

$$S = \frac{\lambda \bar{\lambda} (d + \alpha \hat{\alpha} + 2\alpha^2 r_0^D) - (d + \alpha^2 r_0^D)[2\lambda(1 + 2\lambda) + t^2 \bar{s}_0^D (s_2^R)^2]}{2\lambda \alpha(\alpha[\hat{\alpha} + \alpha r_0^D] - \lambda)},$$

$$\phi = \frac{(d + \alpha^2 r_0^D) \alpha^2 r_0^D P(N_1 > 0, N_2 > 0)}{2\lambda \alpha(\alpha[\hat{\alpha} + \alpha r_0^D] - \lambda)}.$$

Note that in case the destination can successfully receive at most one packet from the aggregators even if both of them transmit, i.e., $r_0^D = 0$, the exact average queueing delay in a node is given by (24) for $\phi = 0$. Moreover, if $r_0^D = r_2^D = 0$, then (24) provides also the exact average delay for the case of a *collision* channel. For the case of the general MPR model where $r_0^D \neq 0$, we can easily obtain bounds for the average delay at aggregators based on the sign of ϕ . Since $P(N_1 > 0, N_2 > 0) > 0$, the sign of ϕ coincides with the sign of $d + \alpha^2 r_0^D$. To proceed, we distinguish the analysis in the following two cases:

- 1) If $d + \alpha^2 r_0^D < 0$, then $0 \leq \phi \leq -\frac{\alpha^2 r_0^D (d + \alpha^2 r_0^D)}{2\lambda\alpha(\alpha[\hat{\alpha} + \alpha r_0^D] - \lambda)}$.

Thus, the upper and lower delay bound, say D_1^{low} , D_1^{up} respectively are,

$$D_1^{low} = S, \quad D_1^{up} = D_1^{low} - \frac{\alpha^2 r_0^D (d + \alpha^2 r_0^D)}{2\lambda\alpha(\alpha[\hat{\alpha} + \alpha r_0^D] - \lambda)}.$$

- 2) If $d + \alpha^2 r_0^D > 0$, then $-\frac{\alpha^2 r_0^D (d + \alpha^2 r_0^D)}{2\lambda\alpha(\alpha[\hat{\alpha} + \alpha r_0^D] - \lambda)} \leq \phi \leq 0$. In such a case,

$$D_1^{up} = S, \quad D_1^{low} = D_1^{up} - \frac{\alpha^2 r_0^D (d + \alpha^2 r_0^D)}{2\lambda\alpha(\alpha[\hat{\alpha} + \alpha r_0^D] - \lambda)}.$$

VI. NUMERICAL RESULTS

In this section, we provide numerical results to evaluate the presented theoretical performance analysis. For exposition convenience, we consider the case where all sensors have the same link characteristics and transmission probabilities.

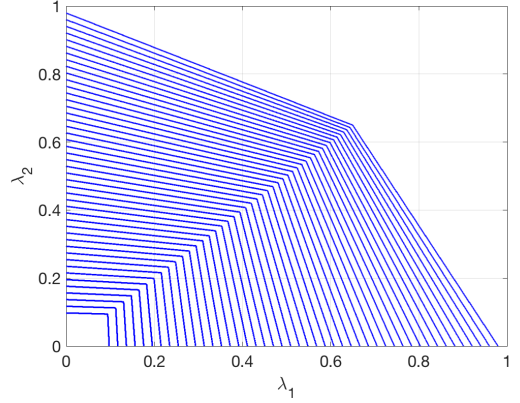
We consider the following network setup, the distance between the sensors and the sink is 130m, the distance between the sensors and the aggregator is 60m, and the distance between the aggregators and the destination is 80m. The path loss exponent is assumed 4, and the transmission power for each sensor is 1mW and for each aggregator is 10mW. We assume Rayleigh block fading channel model. Two values for the SINR threshold are considered in this section, 0.5 and 1.2. In addition, regarding the transmission probabilities of the sensors we consider the values $t = 0.1$ and $t = 0.2$.

A. Stability Region

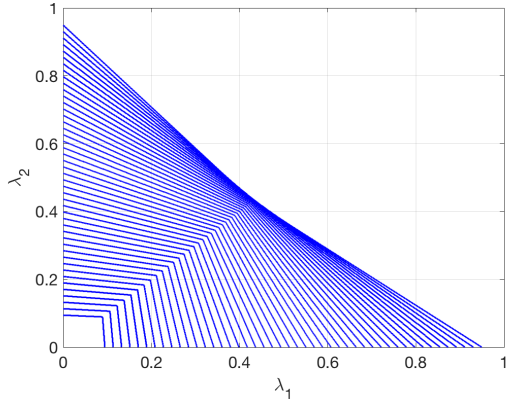
Here we present the closure of the stability region for the queues at the aggregators for all the possible random access probabilities. We consider two cases for the SINR threshold, the case where $SINR = 0.5$, which is depicted in Fig. 2(a). We observe that this region is a convex set, thus, the system performs better than time sharing schemes and this is an indication of strong MPR capabilities at the destination. The stability region for $SINR = 1.2$ is depicted in Fig. 2(b). In this case, a time sharing scheme has higher performance since the destination has weak MPR capabilities.

B. Network Throughput

The throughput per device and the aggregate throughput versus the number of devices covered by an aggregator is depicted in Fig. 3(a) and Fig. 3(b) respectively. We consider two cases for the transmission probabilities of the sensors, $t = 0.2$ and $t = 0.1$. We also plot the throughput of the IoT network without the presence of the aggregators.



(a) $SINR = 0.5$



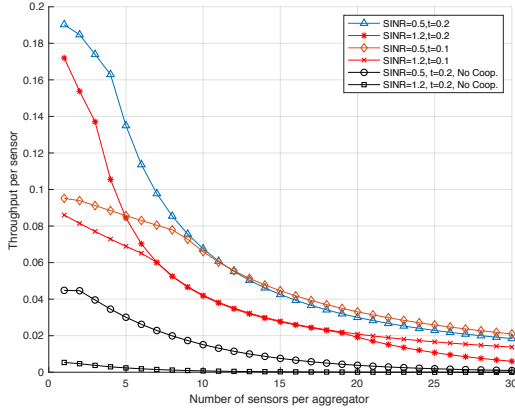
(b) $SINR = 1.2$

Fig. 2. The stability region for the queues at the aggregators.

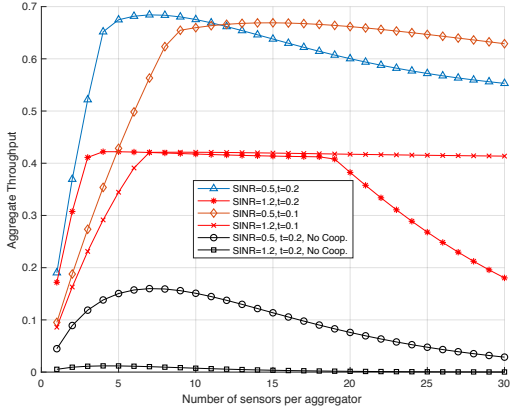
When $SINR = 1.2$ and $t = 0.2$ we observe that the system of the queues is unstable when the number of sensors is between 4 and 18. In this case, as described in Section III, the aggregate throughput is given by the direct throughput plus the service rate of the aggregator. Note that above 19 sensors the system is stable again, the reason behind this phenomenon is that, the aggregators receive more packets than they can support, but after 19 sensors the interference does not allow for a lot of concurrent successful transmissions. *The presence of the aggregators that deploy network-level cooperation provides significant gains in the throughput performance of the network.* These results provide useful guidelines on the number of sensors that can be supported by an aggregator in order to achieve a required network performance.

C. Delay Performance

In Fig. 4, the lower and the upper bounds for the average delay per packet versus the arrival rate at the aggregator are depicted for the two cases of SINR threshold, 0.5 and 1.2 respectively. The values of arrival rates are obtained by the stability conditions and we can connect the value of arrival rate with the number of users and their transmission probability through the expression (3). From that figure, we observe that the average delay for $SINR = 0.5$ is lower than $SINR = 1.2$. It is also important to notice that the upper



(a) Throughput per sensor



(b) Aggregate Throughput

Fig. 3. Throughput performance of the IoT network for various setups.

and the lower bounds are very close, as an indication that the obtained bounds are tight.

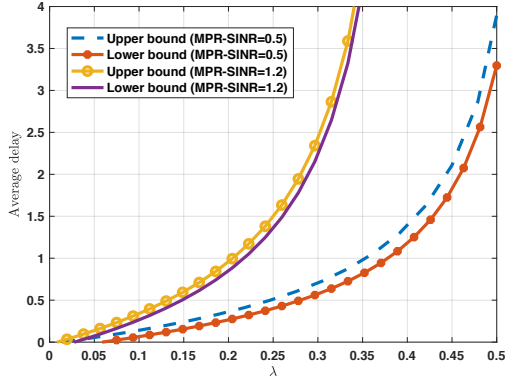


Fig. 4. Delay performance.

VII. SUMMARY AND FUTURE DIRECTIONS

In this work, we considered a random access IoT wireless network assisted by two aggregators providing support for data collection by applying network level cooperation. We characterized the throughput performance of the IoT network and obtained the stability conditions for the queues at the aggregators, which guarantee finite queueing delay. Furthermore,

by applying the theory of boundary value problems we provided a detailed analysis for the delay. Our analytical results provide useful design guidelines for deploying aggregators in random access wireless IoT networks.

The suggested framework in this work can be extended to capture the case of cognitive aggregators that are adapting to the incoming traffic from the sensors and also the channel conditions. In addition, it will be of further interest to consider delay-aware operation protocols for the IoT network and using successive interference cancellation to mitigate interference among the aggregators at the destination. Experimental evaluation of the proposed scheme is also an interesting future research direction.

ACKNOWLEDGEMENTS

This work was supported in part by ELLIIT, Center for Industrial Information Technology (CENIIT), and the Swedish Foundation for Strategic Research.

APPENDIX A

PROOF OF LEMMA IV.1

It is readily seen that $R(x, y) = \frac{xy - \Psi(x, y)}{xy}$, where $\Psi(x, y) = L(x, y)[xy + y(1-x)\alpha_1\hat{\alpha}_2 + x(1-y)\alpha_2\hat{\alpha}_1]$, where for $|x| \leq 1$, $|y| \leq 1$, $\Psi(x, y)$ is a generating function of a proper probability distribution. Now, for $|y| = 1$, $y \neq 1$ and $|x| = 1$ it is clear that $|\Psi(x, y)| < 1 = |xy|$. Thus, a direct application of Rouché's theorem states that, $xy - \Psi(x, y)$ has exactly one zero inside the unit circle. Therefore, $R(x, y) = 0$ has exactly one root $x = X_0(y)$, such that $|x| < 1$. For $y = 1$, $R(x, 1) = 0$ implies

$$(1-x) \left(\lambda_1 + \lambda_1 \frac{\alpha_1 \hat{\alpha}_2 (1-x)}{x} - \frac{\alpha_1 \hat{\alpha}_2}{x} \right) = 0.$$

Therefore, for $y = 1$, and since $\lambda_1 < \alpha_1 \hat{\alpha}_2$, the only root of $R(x, 1) = 0$ for $|x| \leq 1$, is $x = 1$. \square

APPENDIX B

PROOF OF LEMMA IV.3

For $y \in [y_1, y_2]$, $D_y(y)$ is negative, so $X_0(y)$, $X_1(y)$ are complex conjugates. Therefore, $|X(y)|^2 = \frac{\hat{c}(y)}{\hat{a}(y)} = g(y)$. Clearly, $g(y)$ is an increasing function for $y \in [0, 1]$ and thus, $|X(y)|^2 \leq g(y_2) = \beta_0$. Using simple algebraic considerations we can prove that, $X_0(y_1) := \beta_1 = -g(y_1)$ is the extreme left point of \mathcal{M} . Finally, $\zeta(\delta)$ is derived by solving $Re(X(y)) = -\hat{b}(y)/2\hat{a}(y)$ for y with $\delta = Re(X(y))$, and taking the solution such that $y \in [0, 1]$. \square

APPENDIX C

CONSTRUCTION OF THE CONFORMAL MAPPINGS

Our goal in order to obtain expressions for the basic performance metrics is to construct the mapping $\gamma_0(z)$. To proceed, we need a representation of \mathcal{M} in polar coordinates, i.e., $\mathcal{M} = \{x : x = \rho(\phi) \exp(i\phi), \phi \in [0, 2\pi]\}$.

In the following, we summarize the basic steps: Since $0 \in G_{\mathcal{M}}$, for each $x \in \mathcal{M}$, a relation between its absolute value and its real part is given by $|x|^2 = m(Re(x))$ (see Lemma IV.3). Given the angle ϕ of some point on \mathcal{M} , the real part of this point, say $\delta(\phi)$, is the zero of $\delta - \cos(\phi)\sqrt{m(\delta)}$, $\phi \in [0, 2\pi]$. Since \mathcal{M} is a smooth, egg-shaped contour, the solution

is unique. Clearly, $\rho(\phi) = \frac{\delta(\phi)}{\cos(\phi)}$, and the parametrization of \mathcal{M} in polar coordinates is fully specified.

Then, the mapping from $z \in G_C$ to $x \in G_M$, where $z = e^{i\phi}$ and $x = \rho(\psi(\phi))e^{i\psi(\phi)}$, satisfying $\gamma_0(0) = 0$, $\gamma_0(z) = \overline{\gamma_0(\bar{z})}$ is uniquely determined by (see [28], Section I.4.4),

$$\begin{aligned}\gamma_0(z) &= z \exp\left[\frac{1}{2\pi} \int_0^{2\pi} \log\{\rho(\psi(\omega))\} \frac{e^{i\omega} + z}{e^{i\omega} - z} d\omega\right], |z| < 1, \\ \psi(\phi) &= \phi - \int_0^{2\pi} \log\{\rho(\psi(\omega))\} \cot\left(\frac{\omega - \phi}{2}\right) d\omega, 0 \leq \phi \leq 2\pi,\end{aligned}\quad (25)$$

i.e., $\psi(\cdot)$ is uniquely determined as the solution of a Theodorsen integral equation with $\psi(\phi) = 2\pi - \psi(2\pi - \phi)$. This integral equation has to be solved numerically by an iterative procedure. For the numerical evaluation of the integrals we split the interval $[0, 2\pi]$ into M parts of length $2\pi/M$, by taking M points $\phi_k = \frac{2k\pi}{M}$, $k = 0, 1, \dots, M-1$. For the M points given by their angles $\{\phi_0, \dots, \phi_{M-1}\}$ we should solve the second in (25) to obtain the corresponding points $\{\psi(\phi_0), \dots, \psi(\phi_{M-1})\}$, iteratively from,

$$\begin{aligned}\psi_0(\phi_k) &= \phi_k, \\ \psi_{n+1}(\phi_k) &= \phi_k - \frac{1}{2\pi} \int_0^{2\pi} \log\left\{\frac{\delta(\psi_n(\omega))}{\cos(\psi_n(\omega))}\right\} \cot\left[\frac{\omega - \phi_k}{2}\right] d\omega,\end{aligned}\quad (26)$$

where $\lim_{n \rightarrow \infty} \psi_{n+1}(\phi) = \psi(\phi)$, and $\delta(\psi_n(\omega))$ is determined by, $\delta(\psi_n(\omega)) = \cos(\psi_n(\omega))\sqrt{m(\delta(\psi_n(\omega)))}$, using the Newton-Raphson root finding method. For each step, the integral in (26) is numerically determined by again using the trapezium rule with M parts of equal length $2\pi/M$. For the iteration, we have used the following stopping criterion $\max_{k \in \{0, 1, \dots, M-1\}} |\psi_{n+1}(\phi_k) - \psi_n(\phi_k)| < 10^{-6}$

After obtaining $\psi(\phi)$ numerically, the values of the conformal mapping $\gamma_0(z)$, $|z| \leq 1$, can be calculated by applying the Plemelj-Sokhotski formula to the first in (25) for $0 \leq \phi \leq 2\pi$,

$$\gamma_0(e^{i\phi}) = \frac{e^{i\psi(\phi)} \delta(\psi(\phi))}{\cos(\psi(\phi))} = \delta(\psi(\phi)) [1 + i \tan(\psi(\phi))].$$

We can find $\gamma(1)$, $\gamma'(1)$ by applying the Newton's method and solving $\gamma_0(z_0) = 1$, in $[0, 1]$, i.e., z_0 is the zero in $[0, 1]$ of $\gamma_0(z) = 1$. Then, $\gamma(1) = z_0$. Moreover, using the first in (25)

$$\begin{aligned}\gamma'(1) &= (\gamma'_0(z_0))^{-1} \\ &= \left\{ \frac{1}{\gamma(1)} + \frac{1}{2\pi i} \int_0^{2\pi} \frac{\log\{\rho(\psi(\omega))\} 2e^{i\omega}}{(e^{i\omega} - \gamma(1))^2} d\omega \right\}^{-1},\end{aligned}\quad (27)$$

which can be obtained numerically by using the trapezoidal rule for the integral on the right-hand side of (27).

REFERENCES

- [1] J. A. Stankovic, "Research directions for the internet of things," *IEEE Internet of Things Journal*, vol. 1, no. 1, pp. 3–9, Feb 2014.
- [2] V. Angelakis, I. Avgouleas, N. Pappas, E. Fitzgerald, and D. Yuan, "Allocation of heterogeneous resources of an iot device to flexible services," *IEEE Internet of Things Journal*, vol. 3, no. 5, pp. 691–700, Oct 2016.
- [3] A. A. Khan, M. H. Rehmani, and A. Rachedi, "Cognitive-radio-based internet of things: Applications, architectures, spectrum related functionalities, and future research directions," *IEEE Wir. Comm.*, vol. 24, no. 3, pp. 17–25, June 2017.
- [4] M. Hasan, E. Hossain, and D. Niyato, "Random access for machine-to-machine communication in lte-advanced networks: issues and approaches," *IEEE Comm. Mag.*, vol. 51, no. 6, pp. 86–93, June 2013.
- [5] D. Malak, H. S. Dhillon, and J. G. Andrews, "Optimizing data aggregation for uplink machine-to-machine communication networks," *IEEE Trans. on Comm.*, vol. 64, no. 3, pp. 1274–1290, March 2016.
- [6] S. H. Hsu, C. H. Lin, C. Y. Wang, and W. T. Chen, "Minimizing upload latency for critical tasks in cellular-based iot networks using multiple relays," in *IEEE International Conference on Communications (ICC)*, May 2017, pp. 1–7.
- [7] J. Guo, S. Durrani, X. Zhou, and H. Yanikomeroglu, "Massive machine type communication with data aggregation and resource scheduling," *IEEE Trans. on Comm.*, vol. 65, no. 9, pp. 4012–4026, Sept 2017.
- [8] O. L. A. Lopez, H. Alves, P. H. J. Nardelli, and M. Latva-aho, "Aggregation and resource scheduling in machine-type communication networks: A stochastic geometry approach," *IEEE Trans. on Wir. Comm.*, pp. 1–1, 2018.
- [9] T. Salam, W. U. Rehman, and X. Tao, "Cooperative data aggregation and dynamic resource allocation for massive machine type communication," *IEEE Access*, vol. 6, pp. 4145–4158, 2018.
- [10] C. Zhang, J. Ge, M. Pan, F. Gong, and J. Men, "One stone two birds: A joint thing and relay selection for diverse iot networks," *IEEE Trans. on Veh. Tech.*, pp. 1–1, 2018.
- [11] A. Sadek, K. Liu, and A. Ephremides, "Cognitive multiple access via cooperation: Protocol design and performance analysis," *IEEE Trans. Infor. Th.*, vol. 53, no. 10, pp. 3677–3696, Oct 2007.
- [12] B. Rong and A. Ephremides, "Cooperation above the physical layer: The case of a simple network," in *IEEE International Symposium on Information Theory (ISIT)*, 2009, pp. 1789–1793.
- [13] N. Pappas, M. Kountouris, A. Ephremides, and A. Traganitis, "Relay-assisted multiple access with full-duplex multi-packet reception," *IEEE Trans. on Wir. Comm.*, vol. 14, no. 7, pp. 3544–3558, July 2015.
- [14] N. Pappas, M. Kountouris, J. Jeon, A. Ephremides, and A. Traganitis, "Network-level cooperation in energy harvesting wireless networks," in *IEEE Global Conference on Signal and Information Processing*, Dec 2013, pp. 383–386.
- [15] G. Papadimitriou, N. Pappas, A. Traganitis, and V. Angelakis, "Network-level performance evaluation of a two-relay cooperative random access wireless system," *Computer Networks*, vol. 88, pp. 187–201, 2015.
- [16] N. Pappas, M. Kountouris, J. Jeon, A. Ephremides, and A. Traganitis, "Effect of energy harvesting on stable throughput in cooperative relay systems," *Journal of Communications and Networks*, vol. 18, no. 2, pp. 261–269, April 2016.
- [17] I. Dimitriou, "A retrieval queue to model a two-relay cooperative wireless system with simultaneous packet reception," in *International Conference on Analytical and Stochastic Modeling Techniques and Applications*. Springer International Publishing, 2016, pp. 123–139.
- [18] N. Nomikos, T. Charalambous, I. Krikidis, D. N. Skoutas, D. Vouyioukas, M. Johansson, and C. Skianis, "A survey on buffer-aided relay selection," *IEEE Communications Surveys Tutorials*, vol. 18, no. 2, pp. 1073–1097, Secondquarter 2016.
- [19] I. Dimitriou, "A queueing system for modeling cooperative wireless networks with coupled relay nodes and synchronized packet arrivals," *Performance Evaluation*, vol. 114, pp. 16–31, 2017.
- [20] N. Pappas, J. Jeon, D. Yuan, A. Traganitis, and A. Ephremides, "Wireless network-level partial relay cooperation: A stable throughput analysis," *Journal of Communications and Networks*, vol. 20, no. 1, pp. 93–101, Feb 2018.
- [21] I. Dimitriou, "A two-class queueing system with constant retrieval policy and general class dependent service times," *European Journal of Operational Research*, 2018.
- [22] J. Kim, H. K. Lee, D. M. Kim, and S. L. Kim, "Delay performance of two-stage access in cellular internet-of-things networks," *IEEE Trans. on Veh. Tech.*, vol. 67, no. 4, pp. 3521–3533, April 2018.
- [23] S. Verdú, *Multiuser detection*. Cambridge university press, 1998.
- [24] S. Ramakrishnan, *Design of Integrated Full-Duplex Wireless Transceivers*. University of California, Berkeley, 2016.
- [25] R. Rao and A. Ephremides, "On the stability of interacting queues in a multiple-access system," *IEEE Transactions on Information Theory*, vol. 34, no. 5, pp. 918–930, Sep 1988.
- [26] I. Dimitriou and N. Pappas, "Stable throughput and delay analysis of a random access network with queue-aware transmission," *IEEE Trans. on Wir. Comm.*, vol. 17, no. 5, pp. 3170–3184, May 2018.
- [27] G. Fayolle, R. Iasnogorodski, and V. Malyshev, *Random walks in the quarter-plane: Algebraic methods, boundary value problems, applications to queueing systems and analytic combinatorics*. Springer-Verlag, Berlin, 2017.
- [28] J. Cohen and O. Boxma, *Boundary value problems in queueing systems analysis*. Amsterdam, Netherlands: North Holland Publishing Company, 1983.